

## **Structural efficient materials inspired by bamboo with a large, continuous gradient**

*Anran Mao, Jiewei Chen, Xiaochen Bu, Lulu Tian, Weiwei Gao, Eduardo Saiz\* and Hao Bai\**

A. R. Mao, J. W. Chen, X. C. Bu, L. L. Tian, Prof. H. Bai  
State Key Laboratory of Chemical Engineering  
College of Chemical and Biological Engineering  
Zhejiang University  
Hangzhou 310027, China  
E-mail: [hbai@zju.edu.cn](mailto:hbai@zju.edu.cn)

Prof. W. W. Gao  
Department of Polymer Science and Engineering  
Zhejiang University  
Hangzhou 310027, China

Prof. E. Saiz  
Centre for Advanced Structural Ceramics Department of Materials  
Imperial College of London  
London SW7 2AZ, UK  
E-mail: [e.saiz@imperial.ac.uk](mailto:e.saiz@imperial.ac.uk)

**Keywords:** bioinspired material, bamboo, cellular material, 3D printing

**Abstract:** Because of its light weight and high strength, bamboo is used in many applications around the world. Natural bamboo is built from a fiber-reinforced material and exhibits a porous graded architecture that provides its remarkable mechanical performance. This porosity gradient is generated through the unique distribution of densified vascular bundles. Scientists and engineers have been trying to mimic this architecture for a very long time with much of the work focusing on the effect of the fiber reinforcement. However, we still lack quantitative studies on role of the pore gradient design on the mechanical properties, in part because the fabrication of bamboo-inspired graded materials is challenging. Here, we found that Moso bamboo develops a steep and continuous porosity gradient through an ingenious cellular design. We studied systematically the effect of the gradient design on the mechanical performance using 3D printed models, found that not only the magnitude of the gradient but also its continuity has a significant effect. By introducing a continuous and large gradient, the maximum flexural load and energy absorption capability can be increased by 40% and 110% when comparing to the structure without gradient. These bamboo-inspired cellular architectures can offer efficient solutions for the design of damage tolerant engineering structures.

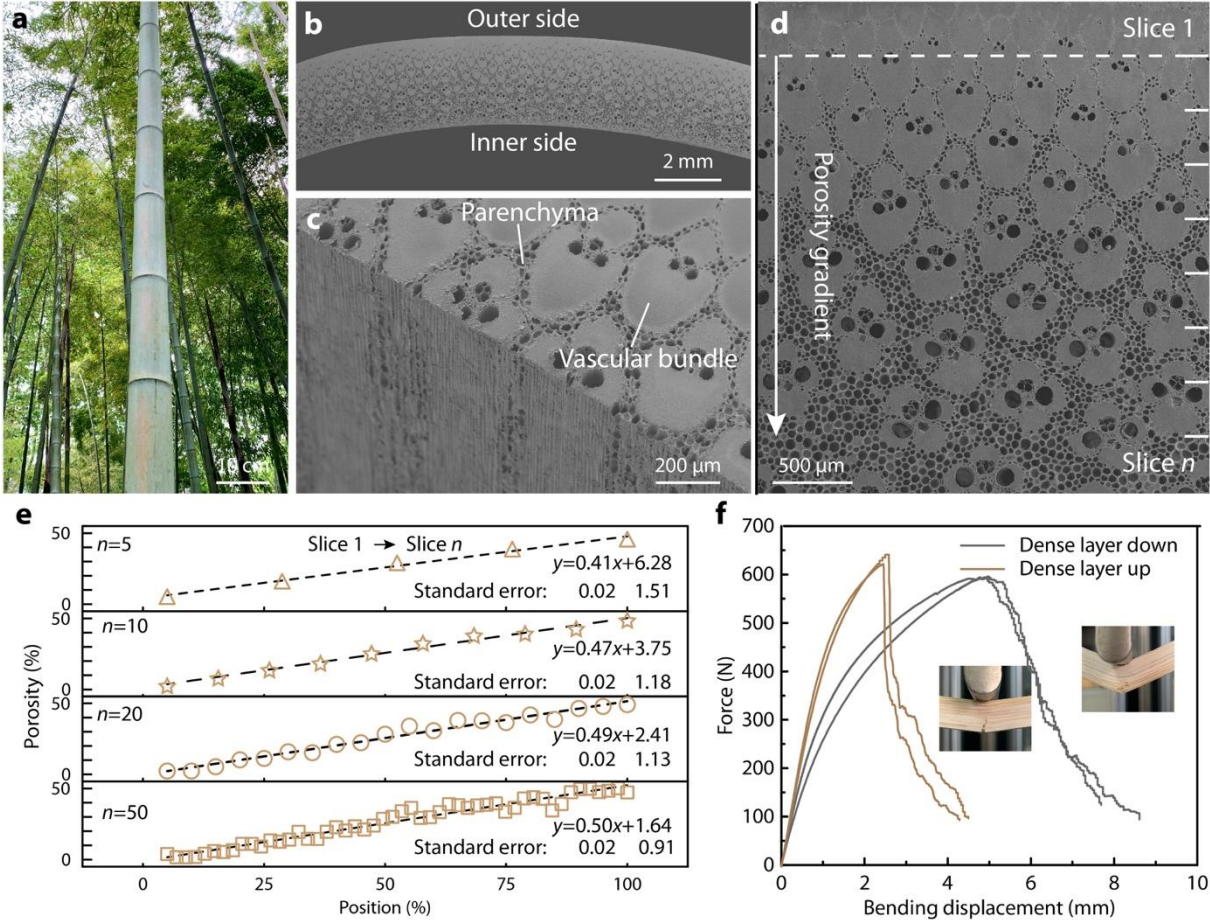
**Introduction:** Nature usually takes advantages of exquisite structural designs to achieve remarkable mechanical performance.<sup>[1-6]</sup> Functional gradients are regarded as one of the basic structural elements widely used in biological materials.<sup>[7]</sup> Bamboo is a prime example of a natural graded composite that has received considerable attention in fundamental scientific research as well as in engineering applications.<sup>[1,8,9]</sup> Different from the gradients in composition or crystal orientation observed in teeth or the lobster exoskeleton, bamboo achieves large porosity gradients through an ingenious cellular structural design<sup>[7]</sup>. Built from a fiber-reinforced material, bamboo consists of densified vascular bundles and porous parenchyma cells aligned in the longitudinal direction.<sup>[10,11]</sup> In contrast to the uniform fiber distribution in woods, there exists a porosity gradient from the outer to the inner side in the cross profile of bamboo.<sup>[12,13]</sup> The failure of natural bamboo has been related to matrix (parenchyma cells) failure, interfacial dissociations and fiber breakage, and the important role of fibers for achieving outstanding mechanical properties has been studied<sup>[11,14,15]</sup>. However, we still lack quantitative studies on the effect of the graded structure on mechanical properties. As the other interesting feature, we would like to discuss the gradient structure itself here. Also, there still remains a vast space for the exploration in the design and fabrication of bamboo-inspired high-performance materials<sup>[16]</sup>. Here, we analyze the graded structure of Moso bamboo, and found that the porosity continuously increases from ~2% at outer side to ~50% at the inner side. We designed and fabricated a series of porous materials by 3D printing, to demonstrate that the large continuous porosity gradients in natural bamboo are beneficial to prevent catastrophic failure and provide a large improvement of the damage tolerance<sup>[17,18]</sup>. These findings could help to develop efficient solutions in the design of advanced light weight structures.

Bamboo (Figure 1a) is a fast-growing plant that usually reaches maturity within years, this is about ten times faster than wood.<sup>[19]</sup> The porous cross section of the bamboo culm (overall porosity about 25~30%) results in a lightweight structure with extraordinary mechanical performance (Figure 1b). The microstructure of bamboo is formed by densified vascular

bundles embedded in porous parenchyma cells (Figure 1c). The vascular bundles consist of fibers that are parallel to the longitudinal direction of the bamboo (Figure S1), and the porous parenchyma consists of honeycomb-like cells with a porosity of about 60%. Previous studies have described the vascular bundle distribution across the thickness of the cross-section<sup>[20]</sup>, as well as the failure mechanism of natural bamboo. <sup>[12,14,20]</sup> However, the relation between microstructural gradients and mechanical behavior is largely unexplored, as it's still challenging to build the comparable counterparts needed to investigate it systematically. In addition, the structural features of bamboo were not fully captured. To analyze the graded structure of bamboo in detail, we extracted a typical cross-section of the bamboo stem including the inner and outer regions (Figure 1d). The porosity gradient is clearly visible. In order to perform a quantitative analysis, we divided the SEM image evenly into  $n$  slices. The slice thicknesses are around 300  $\mu\text{m}$ , 150  $\mu\text{m}$  and 60  $\mu\text{m}$  with  $n=10$ , 20 or 50, respectively. These values are much smaller than the size of individual vascular bundles. Then we used image analysis to calculate the porosity of each slice. The results in Figure 1e show a linear increase in porosity from the outer side to the inner side even when using a large  $n$ , indicating that the gradient is continuous instead of consisting of discrete steps (Table S1). We found that slope of the gradient stabilizes at  $\sim 0.5$  when  $n \geq 20$ . The standard error of the calculated slope is very low (0.02). Thus, we set  $n=20$  in the following study.

Bamboo has been broadly used as structural material and we tested its bending behavior when the tensile face is the dense outer layer and when the tensile face is the porous inner layer (Figure 1f). The measured maximum loads in both cases are very similar although they are slightly higher when the tensile face is in the porous layer. However, the displacement to failure is much larger when the tensile face is in the dense layer suggesting a much larger work of fracture. A dense tensile face will delay crack formation during bending while the porous layers can easily be compressed resulting in a large deformation that contributes to the lower bending modulus and higher flexibility. In addition, once a crack forms, we found that the dense part

promotes stable crack propagation with crack deflection and a more gradual failure increasing the overall work of fracture (inserts in Figure 1f).



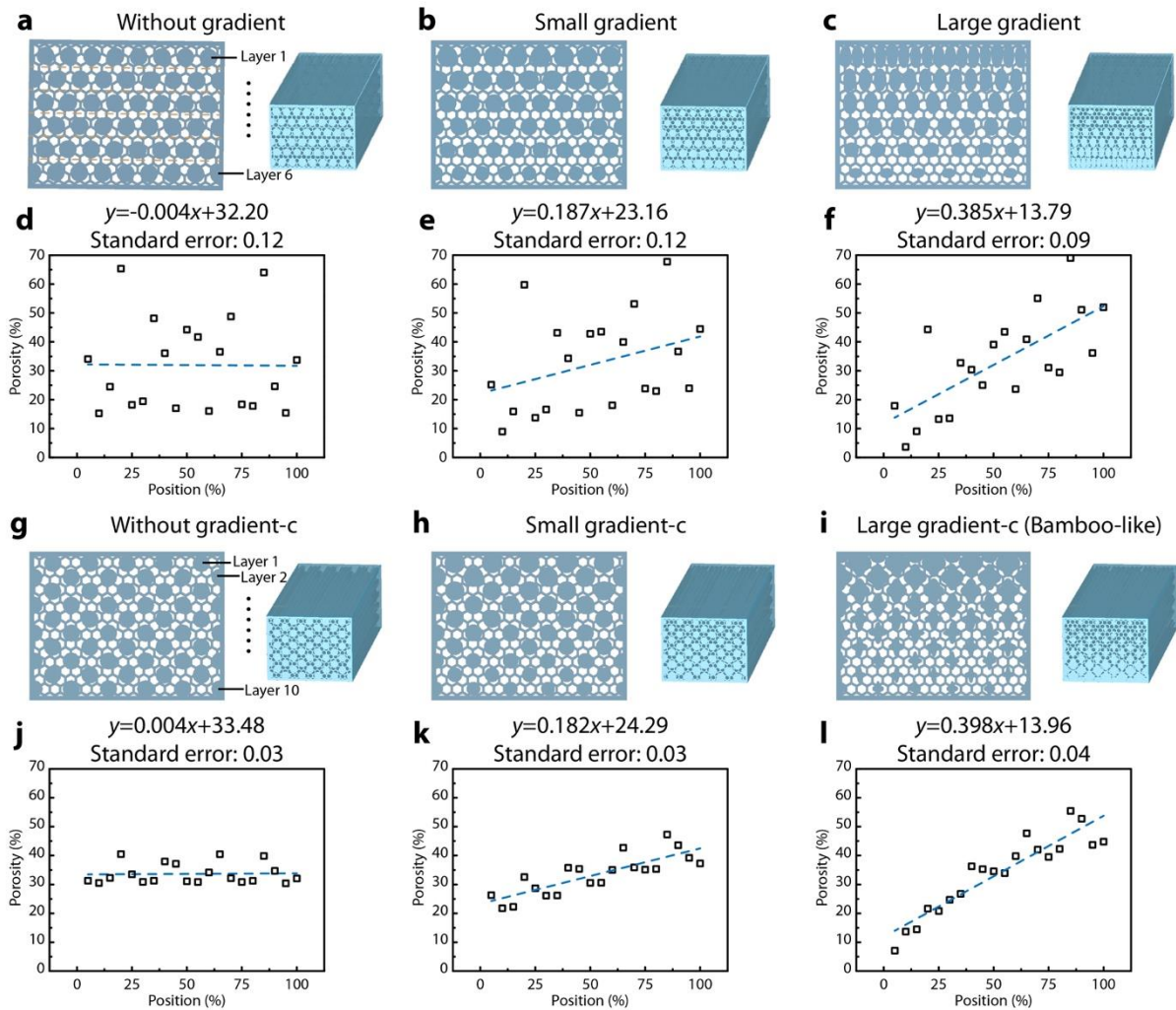
**Figure 1. Architecture and mechanical properties of Moso bamboo.** a) Optical image of the Moso bamboo. b) SEM image of the cross section showing the bamboo is composed of densified vascular bundles and porous parenchyma cells. c) Higher magnification image shows the fibers in the vascular bundles and the parenchyma are aligned in the longitudinal direction of the bamboo. d) The cross-section SEM image of the culm showing a radial porosity gradient from the outer side (more densified) to the inner side (more porous). e) The porosity statistics of the  $n$  slices that evenly divided in (d) showing a continuous gradient. f) Three-point bending test results of the Moso bamboo at two directions.

To confirm the effect of the gradient, we designed six models with different graded porosities (Figure 2). All the models consist of a honeycomb-like porous tissue (porosity: 60%)

which mimics the parenchyma in the natural bamboo, and the dense reinforced parts in the shape of cylinders with round or elliptical cross section that corresponds to the vascular bundles (Figure S2). It's worth to mention that blue color in model design corresponds to the solid part and the white represents the pores. The reinforced parts distribute differently in the honeycomb-like tissue, leading to different porosity gradients. In addition, all models have the same total cross-sectional area of dense material, which results in the same overall porosity of about 28%.

Firstly, we designed three models in which the cross section has a layered structure and the porosity varies from layer to layer in a step-wise fashion. To simplify the structure, we use a cross sectional round shape for the dense reinforcement. Each reinforcement has the same geometry parameter within a layer, and gradually changes in different layers. They are all aligned with the centers placed along a straight line. The basic comparison model is the one “without gradient” (Figure 2a). It consists of six identical layers. The detailed structural parameters of the design can be found in Table S2. In order to quantify the gradient in porosity, we divided the cross section evenly into 20 slices with equal thickness and measure the porosity in each of them (Figure 2d). The fitted straight line exhibits a slope of nearly zero (-0.004), indicating there is no gradient. However, the chart (Figure 2d) shows a large variation in the porosity as there is no overlap between adjacent layers, and the slices used for the image analysis are much thinner than the diameter of dense parts. We chose 20 slices here due to the standard error in the linear fitting of porosity is basically stable even the number of slices further increases (Figure S3). Similarly, we designed “small gradient” and “large gradient” models (Figure 2b, c). In all three models the porosity changes step-wise, from slice to slice, which results in a large standard error in the slope (about 0.09~0.12) compared to that of natural bamboo (0.02). For the “small gradient” model, the porosity varies gradually, as shown in Figure 2b. The corresponding porosity-position relationship exhibits a slope of 0.187 (Figure 2e). To achieve the high density in one of the sides of the “large gradient” model, we used dense

regions with an oval shape. The results in Figure 2f show a much larger slope, which reveals the large degree of variation in porosity from side to side.

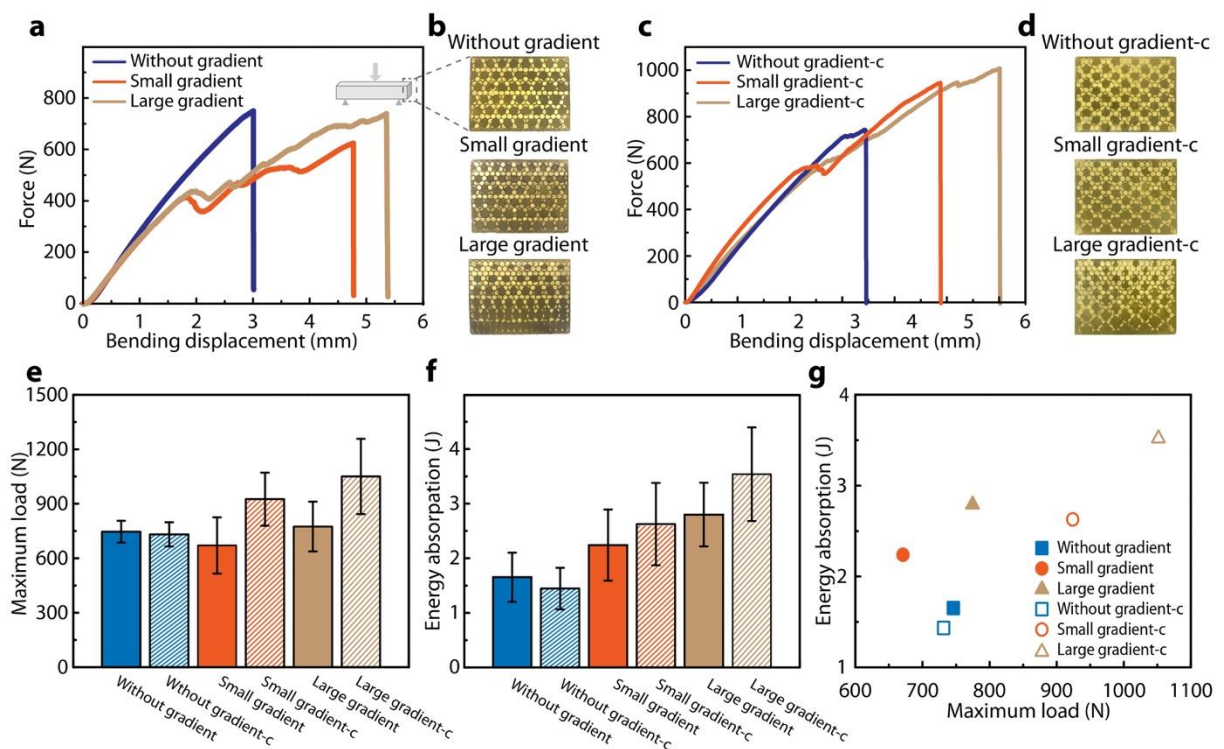


**Figure 2. CAD design and the porosity statistics of the biomimetic models.** a-c) The cross-section images of three models with different porosity gradients (without gradient, small gradient, large gradient, respectively) through discontinuous distribution way. d-f) The porosity statistics of the models in a-c. g-i) The cross-section images of three models with different porosity gradients through continuous distribution way. j-l) The porosity statistics of the models in g-i. In which the large gradient-continuous model is the most similar to the natural Moso bamboo structure.

The second set of models (Figure 2g-i) exhibit a more continuous gradient achieved by overlapping the dense regions. The standard errors in the measured graded slope are about 0.03-0.04, which are much lower than the models in Figure 2a-c. The corresponding detailed structural parameters can be found in Table S3. In order to achieve a continuous gradient by layer overlapping, we design three models consisting of ten layers to reduce interlayer spacing. Specifically, the “without gradient-continuous” (without gradient-c) model exhibits a slope of 0.004 which is nearly zero, this confirms it can be regarded as a model with no gradient (Figure 2j). Similar slope can also be found in the small gradient and small gradient-c, large gradient and large gradient-c (Figure 2k, l). As for the “large gradient-c” model (Figure 2i), to further increase the density of the top part, we combined two ovals in a cross pattern to form the dense region (Figure S4). This cross pattern is also similar to the shape of vascular bundles in Figure 1d. The slope of this model is 0.398, approaching that of natural bamboo (0.49) (Figure 2l). Similarly, we also analyzed the standard error of “large gradient-c” model when it’s divided into different number of slices (Figure S5). The results further confirmed the much smaller standard error when compared with “without gradient” model, which demonstrated the “large gradient-c” is more continuous. Based on the similar slope and standard error with natural bamboo, we regarded the “large gradient-c” model as the bamboo-like model, due to the structural similarity.

To study the effect of structure, we fabricated the six models by Digital Light Processing (DLP) with photo-curable resin (specific information can be found in Experimental Section)<sup>[21-27]</sup>. According to the different bending behaviors observed in natural bamboo (Figure 1f.), we placed the dense region in the tensile face as to reach higher energy absorption (Figure 3b, d). We first compared the three-point bending results of the models with discrete porosities. The “without gradient” material exhibits the lowest displacement before fracture and a load-displacement curve that raises smoothly until a sudden, catastrophic failure occurs (Figure 3a). In the models with “small” and “large” gradients, the maximum displacement increases as the

porosity gradient increases. However, the maximum load of the graded model does not show an obvious improvement. Meanwhile, a linear increase in the load-displacement curve is followed by fluctuations that start at about 2 mm displacement. We consider this should be related to the buckling of the pore walls in the material. As in bamboo when the gradient is introduced, the porous upper side under compression is more deformable, leading to the higher fracture displacement. It's worth to mention we use force-displacement line instead of stress-strain line here because the equation  $\sigma = \frac{3FL}{2bd^2}$  ( $F$  is the applied force,  $L$  is span,  $b$  is the width of sample,  $d$  is the thickness of sample) which derives from  $\sigma = \frac{Mc}{I}$  ( $I$  is the moment of inertia,  $M$  is the bending moment,  $c$  is the distance from the neutral axis) is only suitable for homogenous rectangular sample. Here, all the designed models have a graded structure with complex design which cannot directly calculate the stress with above equation. Since all the samples have same size and same density, it's reasonable to compare the maximum load and displacement directly.





**Fig. 3. Performance tests of the designed models.** a) The three-point bending test results of the discontinuous models with different porosity gradients. b) The optical images of the cross-section of samples in (a). c) The three-point bending test results of the continuous models with different porosity gradients. d) The optical images of the cross-section of samples in (c). e) The maximum loads of the designed models in three-point bending tests. f) The energy absorption of the designed models. g) Summary of the energy absorption and maximum load. The bamboo-like (large gradient-c) model exhibits superior mechanical properties than the other models. Error bars represent standard deviations calculated from at least five specimens.

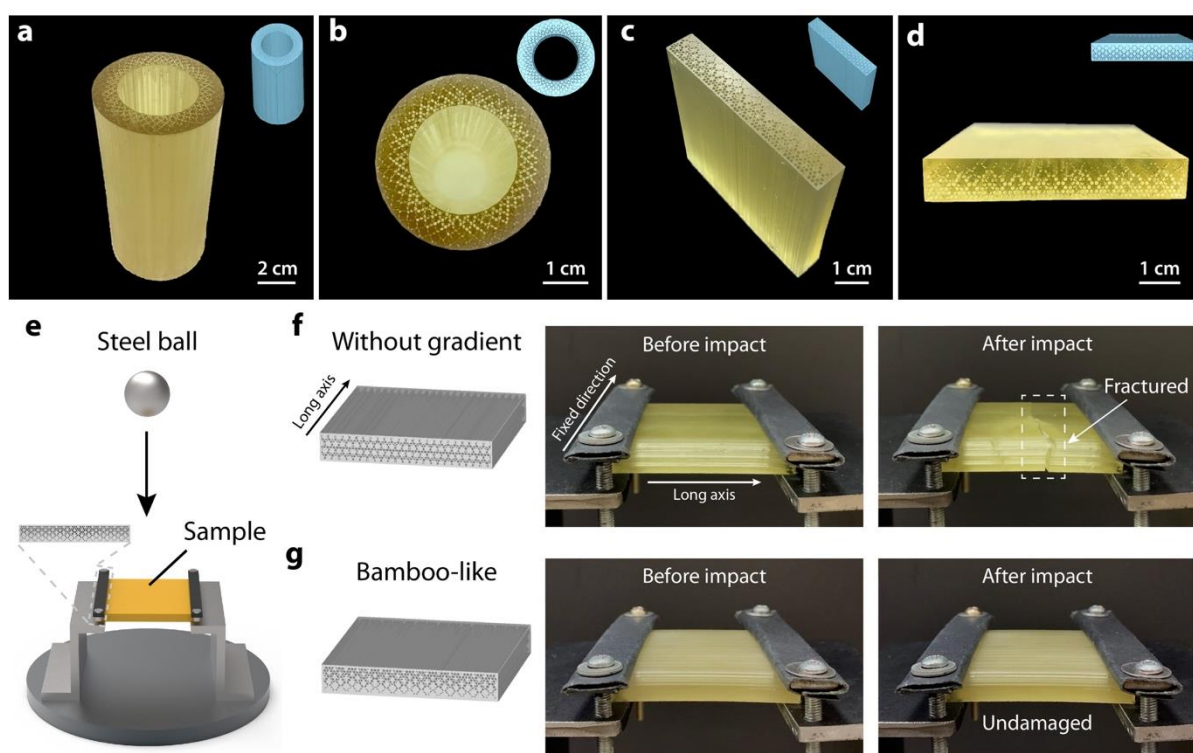
Since the role of the gradient slope has been confirmed in the previous experiments, we investigated the effect of the continuity. The maximum load is largely improved by increasing the continuity (Figure 3c). The gradient slope has a similar effect with the one observed in the previous model. The “without gradient-c” exhibits the smallest fracture displacement, and a smooth load-displacement behavior. When the gradient becomes steeper, both the displacement at fracture and the maximum load increase. Figure 3e, f summarizes the maximum loads and energy absorption (calculated by the integrated area under the force-displacement line) in the different models. On the whole, both the maximum load and the energy absorption increase as the gradient becomes steeper and more continuous. This is further confirmed in the chart in Figure 3g (Table S4). The bamboo-like model exhibits the best performance, confirming the structural advantages of natural bamboo.

To better understand the underlying mechanism, we conducted Finite Element Analysis to simulate the stress distribution in the six models during three-point bending (Figure S7). We applied same displacement in different models, and extracted the cross-section of the model for better observation. As expected, the area under the top pin exhibits high compressive stresses, and the bottom side shows a high tensile stress. Failure usually initiates at the tensile side close to the area of maximum stress. In the three models with no continuity (Figure S7a-c), we found that, for the same displacement, the maximum stress at the bottom decreases gradually when

the gradient increases. This means that they will require more bending to reach failure which increases the flexibility of the structure. Similar effects have been observed before in porous graded materials.<sup>[28]</sup> Here we show that not only the magnitude of the gradient but also its continuity has an effect. When a more continuous gradient is used, the maximum stress decreases further (Figure S7d-f). The reduced tensile stress at the bottom side is beneficial to improve the maximum load to fracture. In addition, there may be other effects as the force-displacement curves (Figure 3 a) suggest that fluctuation caused by internal wall failure (e.g. buckling) may decrease the maximum load that can be reached in structures with a less continuous gradient, whereas the force drop in samples with a continuous gradient during loading are relatively small (Figure 3 c). In conclusion, the bamboo-like (“large gradient-c”) structure with a steeper and more continuous gradient in porosity exhibits larger displacement at failure and maximum load.

We translated the design principles learned from the model gradients to bamboo-like materials with more complex shapes. For example, we designed bamboo-like models with a hollow cylinder shape, and fabricated them by 3D printing (Figure 4a, b). As shown in Figure 4a, the material not only mimics the macroscopic hollow cylinder shape of natural bamboo, but also mimics its microstructural features: large and continuous porosity gradient (Figure 4b). To expand the use of this structure, we also designed a bamboo-like plate material, and fabricated it by 3D printing. The optical images show a 60 mm×60 mm×10 mm plate, this can be changed due to demands (Figure 4c). The cross-section shows that this is a six-layer plate material with an obvious porosity gradient (Figure 4d). To assess the mechanical performance of the bamboo-like plate material, we designed an impact test device, in which the samples are fixed on the stage with the more porous part on the top, and a steel ball of 260 g weight is dropped on them from a height of 1.5 m (Figure 4e). To demonstrate the impact resistance of the graded structure, we also designed a homogeneous plate (no gradient in porosity) for comparison. The structure of the two models can be found in Figure 4f, g, respectively. Firstly, we put the long axis of the

pores perpendicular with the grips (fixed direction). The bamboo-like plate material remains undamaged after impact, while the homogeneous plate fractures (Movie S1). To investigate the impact performance of the samples in the other direction, we rotate it 90° horizontally and put long axis of the densified parts parallels to the grips (Figure S8). Results are similar, the homogeneous plate fractures while the bamboo-like material remains intact (Movie S2). Due to its outstanding performance, light-weight bamboo-like structures can be of great interest for many structural applications.



**Fig. 4. Demonstration of the bamboo-like materials.** a, b) Optical images of a tubular bamboo-like material. c, d) Optical images of a plate with a bamboo-like structure. e) Schematic of the impact test device. f) The impact test results of the “without gradient” material. g) The impact test results of bamboo-like material in the direction that long axis of the pores is perpendicular to the grips.

In conclusion, we studied the unique architecture of natural bamboo, characterized by densified vascular bundles embedded in the porous parenchyma. This structure exhibits a large and highly continuous porosity gradient. We investigated systematically the influence of this

gradient using 3D printed models, and found that a large and continuous gradient enables higher bending loads and enhances flexibility. These features result in mechanically efficient structures with an improved flexural resistance, impact resistance and energy absorption capabilities. We could integrate these design principles into tailored shapes which could be potentially used in light weight structural applications in construction or transportation or for energy absorption.

## **Experimental Section**

*Materials:* Moso bamboos were purchased at the local markets in Hangzhou, China. Bisphenol A epoxy acrylate (RJ313) was purchased from RYOJI Chemical Co., Ltd, Germany. The 1,6-Hexanediol diacrylate (HDDA) and Phenylbis(2,4,6-trimethylbenzoyl) phosphine oxide were purchased from Shanghai Macklin Biochemical Co., Ltd, China. The UV-curable polymer precursor solution was prepared by mixing RJ313 and HDDA at a ratio of 50:50 in weight. Phenylbis(2,4,6-trimethylbenzoyl) phosphine oxide was added at the concentration of 1.5 wt% of the precursor solution as the photoinitiator.

*Structural Characterization and Analysis:* Structural characterization specimens were cut from the center positions of the bamboo internodes stalks. The morphology of the bamboo was collected on a field-emission SEM instrument (SU-3500, Hitachi, Tokyo, Japan) at an acceleration voltage of 5 kV. The structural analysis including the porosity calculation and statistics were performed with Image J software. Specifically, we first divided the image of the bamboo into several equal parts by a program design. And then imported them into the Image J, a binarization threshold was setted and porosities were calculated.

*Model Design and 3D-Printing:* The six biomimetic models including the bamboo-like models were created by using a computer-aided design (CAD) application. They were fabricated with the as prepared UV-curable polymer precursor solution by a Digital Light Processing (DLP) 3D printer (Phoenix Touch Pro, FSL 3D, USA). The cured resin has a typical elastic modulus of 200 MPa and a bending strength of about 22 MPa (Figure S6). The exposure time was 0.9 s. Printed models were rinsed in ethanol for 30 s for 3 times to remove any uncured precursor solution. All the samples were printed under the same condition.

*Mechanical Characterization and Simulation:* Bending tests were performed with an Instron 5944. For the bending test of natural bamboo, the samples size was 7 mm × 8 mm × 60 mm with the support span of 42 mm. As for the three-point bending test, the size of the printed samples is 15 mm × 20 mm × 60 mm, with the support span of 45 mm. The specimens were tested at a

strain rate of  $0.015 \text{ mm s}^{-1}$ . A minimum of five specimens were tested for each sample. In the impact tests, the size of the bamboo-like material and without gradient material is  $60 \text{ mm} \times 60 \text{ mm} \times 10 \text{ mm}$ . They were studied by dropping a steel ball with 260 g in weight from a height of 1.5 m. FEM simulations were performed with the ABAQUS program. The stress distributions of 3D models were simulated by importing the model built from the CAD application into ABAQUS. The boundary condition is set to a displacement of 2 mm. The modulus of the material was set to 200 MPa.

### **Acknowledgements**

This work was supported by the National Natural Science Foundation of China (Grant Nos. 22075244, 51722306, and 21674098), Shanxi-Zheda Institute of Advanced Materials and Chemical Engineering (Grant No. 2021SZ-TD009), State Key Laboratory of Chemical Engineering grant SKL-ChE-20T06, the China Scholarship Council (CSC, No:202106320173).

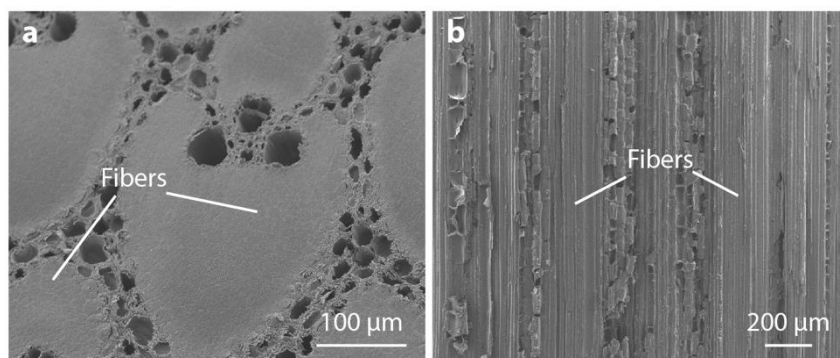
## References

- [1] U. G. K. Wegst, H. Bai, E. Saiz, A. P. Tomsia, R. O. Ritchie, *Nat. Mater.* **2014**, *14*, 23.
- [2] P. Fratzl, R. Weinkamer, *Progress in Materials Science* **2007**, *52*, 1263.
- [3] M. Eder, S. Amini, P. Fratzl, *Science* **2018**, *362*, 543.
- [4] M. A. Meyers, J. McKittrick, P. Y. Chen, *Science* **2013**, *339*, 773.
- [5] L. J. Gibson, M. F. Ashby, *Cellular Solids: Structure & Properties*, Cambridge University Press, **1997**.
- [6] J. Aizenberg, J. C. Weaver, M. S. Thanawala, V. C. Sundar, D. E. Morse, P. Fratzl, *Science* **2005**, *309*, 275.
- [7] Z. Liu, M. A. Meyers, Z. Zhang, R. O. Ritchie, *Progress in Materials Science* **2017**, *88*, 467.
- [8] U. G. Wegst, *J Mech Behav Biomed Mater* **2011**, *4*, 744.
- [9] K. Yin, M. D. Mylo, T. Speck, U. G. K. Wegst, *J Mech Behav Biomed Mater* **2020**, *110*.
- [10] Z.-P. Shao, C.-H. Fang, S.-X. Huang, G.-L. Tian, *Wood Science and Technology* **2009**, *44*, 655.
- [11] S. Amada, S. Untao, *Composites: Part B* **2001**, *32*, 451.
- [12] M. K. Habibi, A. T. Samaei, B. Gheshlaghi, J. Lu, Y. Lu, *Acta Biomaterialia* **2015**, *16*, 178.
- [13] T. Tan, N. Rahbar, S. M. Allameh, S. Kwofie, D. Dissmore, K. Ghavami, W. O. Soboyejo, *Acta Biomater.* **2011**, *7*, 3796.
- [14] G. Chen, H. Luo, H. Yang, T. Zhang, S. Li, *Acta Biomater.* **2018**, *65*, 203.
- [15] J. Q. Krause, F. de Andrade Silva, K. Ghavami, O. d. F. M. Gomes, R. D. T. Filho, *Construction and Building Materials* **2016**, *127*, 199.
- [16] P. G. Dixon, J. T. Muth, X. Xiao, M. A. Skylar-Scott, J. A. Lewis, L. J. Gibson, *Acta Biomater* **2018**, *68*, 90.
- [17] A. Velasco-Hogan, J. Xu, M. A. Meyers, *Adv. Mater.* **2018**, *30*, 1800940.
- [18] Y. Yang, X. Song, X. Li, Z. Chen, C. Zhou, Q. Zhou, Y. Chen, *Adv. Mater.* **2018**, *1706539*.
- [19] M. K. Habibi, Y. Lu, *Sci. Rep.* **2014**, *4*, 5598.
- [20] K. Ghavami, C. S. Rodrigues, S. Paciornik, **2003**.
- [21] G. X. Gu, M. Takaffoli, M. J. Buehler, *Adv. Mater.* **2017**, *29*, 1700060.
- [22] B. G. Compton, J. A. Lewis, *Adv. Mater.* **2014**, *26*, 5930.
- [23] J. R. Raney, B. G. Compton, J. Mueller, T. J. Ober, K. Shea, J. A. Lewis, *Proc. Natl Acad. Sci. USA* **2018**, *115*, 1198.
- [24] A. R. Studart, *Chem. Soc. Rev.* **2016**, *45*, 359.
- [25] M. M. Porter, D. Adriaens, R. L. Hatton, M. A. Meyers, J. McKittrick, *Science* **2015**, *349*, aaa6683.

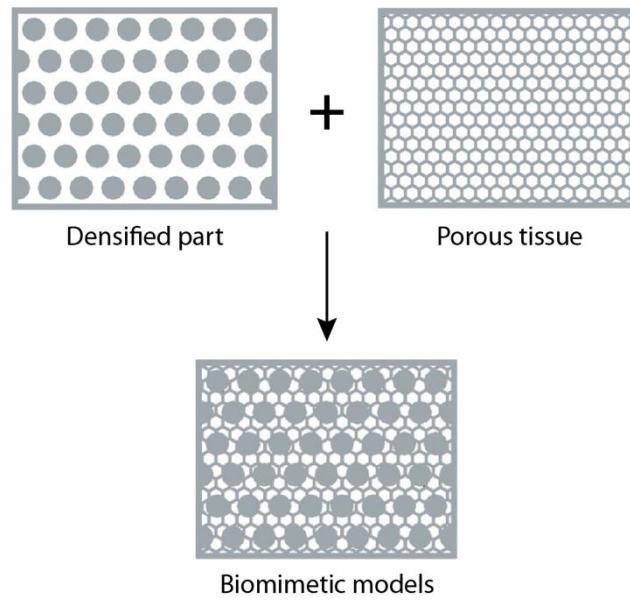
- [26] A. Mao, N. Zhao, Y. Liang, H. Bai, *Adv. Mater.* **2021**, *33*, 2007348.
- [27] M. C. Fernandes, J. Aizenberg, J. C. Weaver, K. Bertoldi, *Nat Mater* **2021**, *20*, 237.
- [28] N. Gupta, S. K. Gupta, B. J. Mueller, *Mater. Sci. Eng. A* **2008**, *485*, 439.



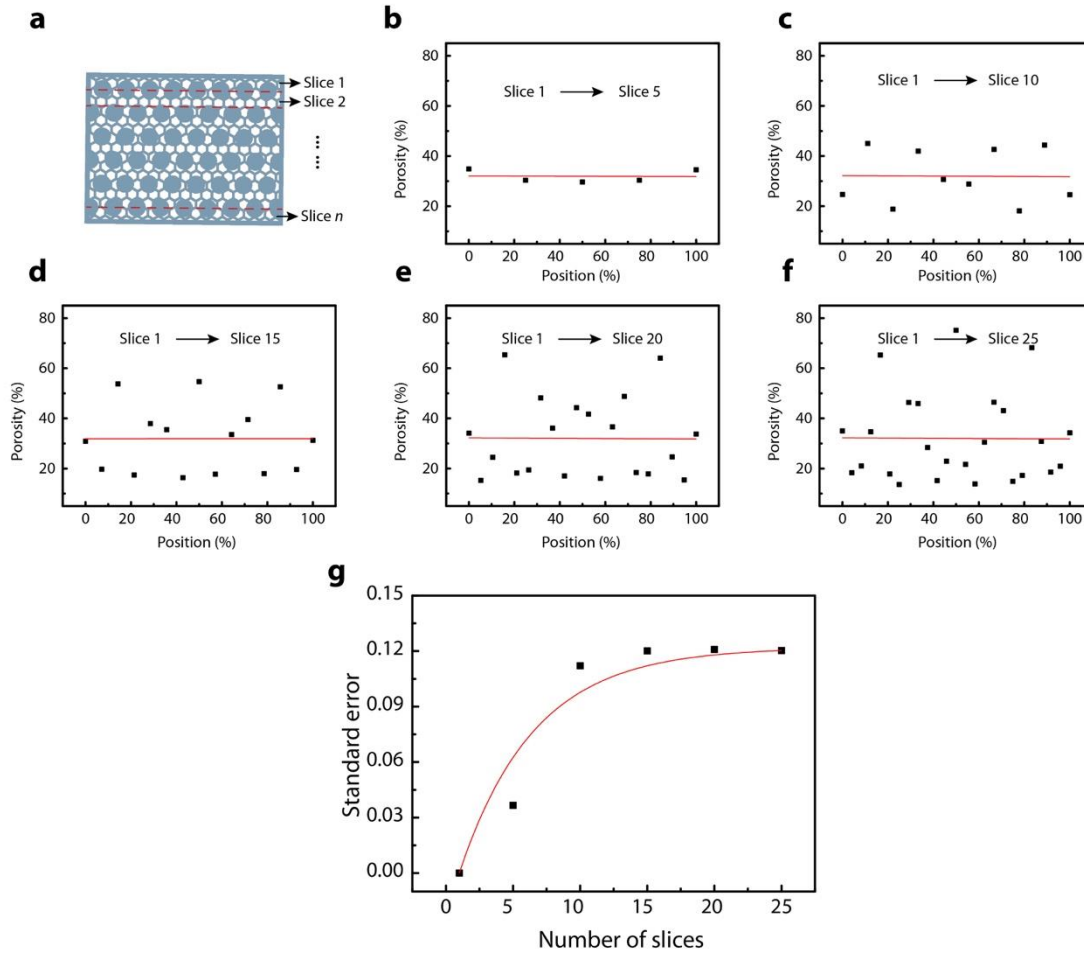
## Supporting Information



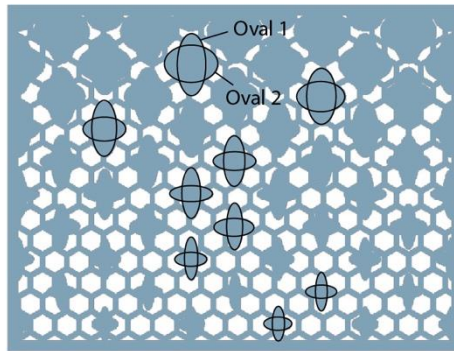
**Figure S1.** SEM images of the cross section and longitudinal section of bamboo with higher magnification.



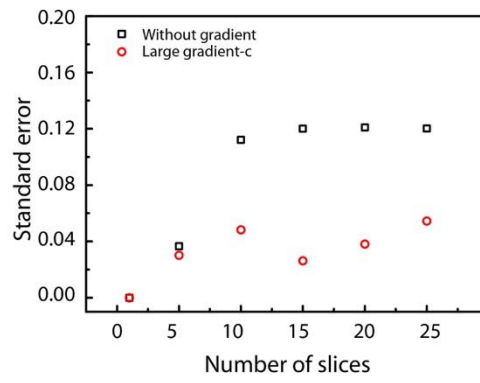
**Figure S2.** The design process of the biomimetic models, indicating the densified parts are embedded in the honeycomb-like porous tissue.



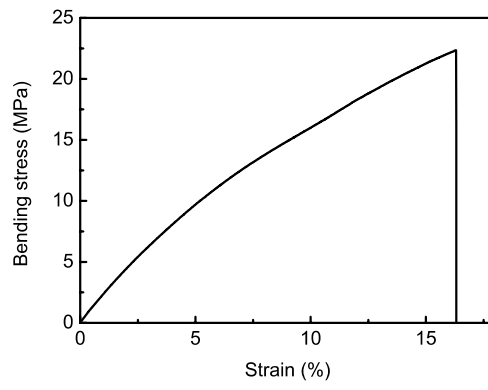
**Figure S3. The porosity statistics of “without gradient” model.** a) The cross section of the model evenly divided into  $n$  slices. b) The porosity statistic of each slice when the model is divided into 5 slices ( $n=5$ ). c-f) the porosity statistics when divided into 10, 15, 20, 25 slices, respectively. g) The standard error of the linear fitting line in b-f.



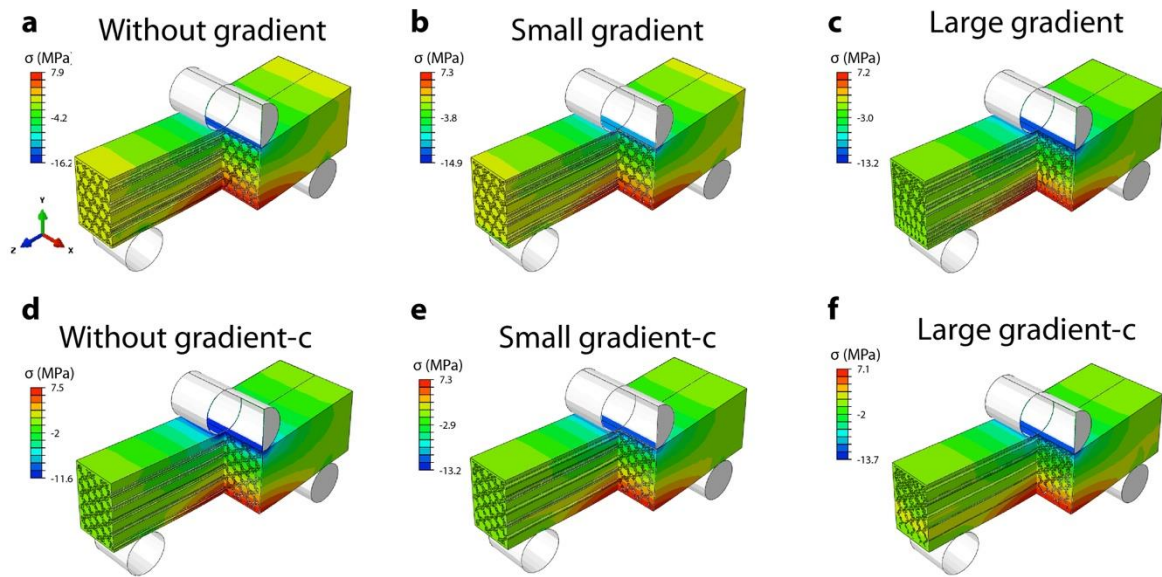
**Figure S4.** The design of the Large gradient-c model exhibits each densified part consists of two overlapped ovals.



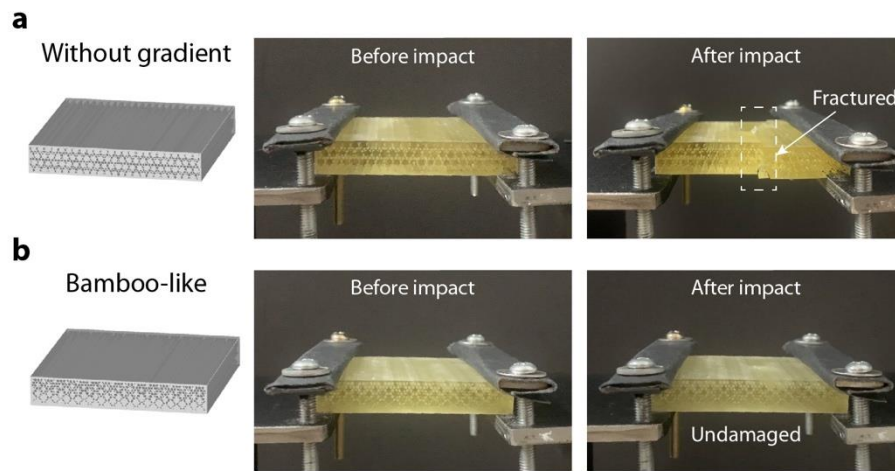
**Figure S5.** The standard error of linear fitting in porosity statistics of “without gradient” model and “large gradient-c” model when the cross section is divided into different slices.



**Figure S6.** The three-point bending results of the 3D printed solid specimen with pure resin.



**Figure S7. Finite element simulation studies on the mechanics of the continuous and large gradient porosity of bamboo.** a-f) The three-point bending simulation results of the maximum principal stress distribution in z direction of without gradient, small gradient, large gradient, without gradient-c, small gradient-c, large gradient-c models, respectively. The boundary condition is set to a displacement of 2 mm.



**Figure S8.** The impact test results of the without gradient material and bamboo-like material in the direction that long axis parallels to the fixed direction.



**Table S1** | Summary of the porosity of each layer in natural bamboo.

| Slice | Position (%) | Porosity (%) |
|-------|--------------|--------------|
| 1     | 5            | 2.58         |
| 2     | 10           | 2.62         |
| 3     | 15           | 5.60         |
| 4     | 20           | 10.45        |
| 5     | 25           | 11.47        |
| 6     | 30           | 16.12        |
| 7     | 35           | 15.46        |
| 8     | 40           | 21.37        |
| 9     | 45           | 22.50        |
| 10    | 50           | 28.52        |
| 11    | 55           | 34.23        |
| 12    | 60           | 30.98        |
| 13    | 65           | 38.23        |
| 14    | 70           | 37.98        |
| 15    | 75           | 36.69        |
| 16    | 80           | 42.12        |
| 17    | 85           | 38.91        |
| 18    | 90           | 46.65        |
| 19    | 95           | 48.04        |
| 20    | 100          | 49.35        |

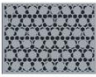
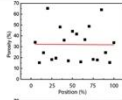

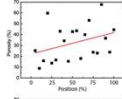

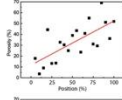

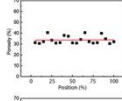

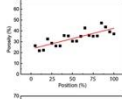

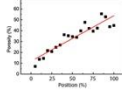
**Table S2** | Summary of the structure parameters of densified parts in without gradient, small gradient and large gradient models.

| Layer | Without gradient | Small gradient | Large gradient     |                     |
|-------|------------------|----------------|--------------------|---------------------|
|       | Diameter         | Diameter       | Long axis diameter | Short axis diameter |
| 1     | 0.76             | 0.87           | 0.98               | 0.49                |
| 2     | 0.76             | 0.83           | 0.97               | 0.55                |
| 3     | 0.76             | 0.78           | 0.93               | 0.62                |
| 4     | 0.76             | 0.73           | 0.79               | 0.63                |
| 5     | 0.76             | 0.68           | 0.63               | 0.63                |
| 6     | 0.76             | 0.62           | 0.44               | 0.58                |

**Table S3** | Summary of the structure parameters of densified parts in without gradient-c, small gradient-c and large gradient-c models.

| Layer | Without gradient-c | Small gradient-c | Large gradient-c   |                     |                    |                     |
|-------|--------------------|------------------|--------------------|---------------------|--------------------|---------------------|
|       | Diameter           | Diameter         | Oval 1             |                     | Oval 2             |                     |
|       |                    |                  | Long axis diameter | Short axis diameter | Long axis diameter | Short axis diameter |
| 1     | 0.74               | 0.87             | 1.20               | 0.60                | 1.05               | 0.80                |
| 2     | 0.74               | 0.85             | 1.15               | 0.55                | 1.00               | 0.70                |
| 3     | 0.74               | 0.82             | 1.10               | 0.55                | 0.90               | 0.60                |
| 4     | 0.74               | 0.79             | 1.05               | 0.50                | 0.80               | 0.44                |
| 5     | 0.74               | 0.76             | 1.00               | 0.40                | 0.80               | 0.36                |
| 6     | 0.74               | 0.73             | 0.95               | 0.35                | 0.80               | 0.30                |
| 7     | 0.74               | 0.70             | 0.85               | 0.30                | 0.70               | 0.35                |
| 8     | 0.74               | 0.67             | 0.80               | 0.25                | 0.60               | 0.30                |
| 9     | 0.74               | 0.63             | 0.70               | 0.24                | 0.55               | 0.25                |
| 10    | 0.74               | 0.59             | 0.65               | 0.22                | 0.50               | 0.30                |

**Table S4** Summary of mechanical behavior of the 3D printed models.

| Model                          | Maximum load (N) | Energy absorption (J) | Pattern   | Porosity gradient   | Linear fitting    | Standard error |           |
|--------------------------------|------------------|-----------------------|---|---|-------------------|----------------|-----------|
|                                |                  |                       |   |   |                   | Slope          | Intercept |
| Without gradient               | 746.1            | 1.65                  |  |  | $y=-0.004x+32.20$ | 0.12           | 7.07      |
| Small gradient                 | 670.8            | 2.24                  |  |  | $y=0.187x+23.16$  | 0.12           | 6.85      |
| Large gradient                 | 774.5            | 2.80                  |  |  | $y=0.385x+13.79$  | 0.09           | 5.27      |
| Without gradient-c             | 731.5            | 1.45                  |  |  | $y=0.004x+33.48$  | 0.03           | 1.57      |
| Small gradient-c               | 925.4            | 2.63                  |  |  | $y=0.182x+24.29$  | 0.03           | 1.77      |
| Large gradient-c (Bamboo-like) | 1050.1           | 3.54                  |  |  | $y=0.398x+13.96$  | 0.04           | 2.22      |